

Comparison of PbI_2 and HgI_2 for direct detection active matrix x-ray image sensors

R. A. Street,^{a)} S. E. Ready, K. Van Schuylenbergh, J. Ho, J. B. Boyce, and P. Nylen^{b)}
Xerox PARC, 3333 Coyote Hill Road, Palo Alto, California 94304

K. Shah
RMD, Watertown, Massachusetts 02172

L. Melekhov and H. Hermon
Real-time Radiography, Jerusalem, Israel

(Received 2 August 2001; accepted for publication 20 November 2001)

The factors determining the x-ray sensitivity of HgI_2 and PbI_2 as direct detector materials for large area matrix addressed x-ray image sensors are described, along with a model to explain their different properties. The imaging studies are made on test arrays with 512×512 pixels of size $100 \mu\text{m}$. The x-ray sensitivity and spatial resolution are reported, along with measurements of the various mechanisms that influence the sensitivity, such as charge collection, x-ray absorption, fill factor, and image lag. The spatial resolution of PbI_2 decreases with increasing film thickness, but this effect is not observed in HgI_2 . The x-ray response data are used to compare the sensitivity to the theoretical values for the ionization energy and to identify the various loss mechanisms. We find that the sensitivity of HgI_2 can be explained by a few small and well characterized loss factors. This material exhibits good spatial resolution, high fill factor, and high charge collection. PbI_2 films exhibit lower sensitivity, principally attributable to a very large image lag. We propose that the x-ray response of the two materials is distinguished by their different depletion layer properties, and present a model that accounts for the sensitivity, image lag, and spatial resolution of PbI_2 . © 2002 American Institute of Physics. [DOI: 10.1063/1.1436298]

I. INTRODUCTION

Large area matrix-addressed image sensor arrays are a recent technology for x-ray imaging, with medical diagnostic and other applications.¹ Two modes of detection are used, either detecting the emission from a phosphor with a photodiode light sensor (indirect detection), or using a thick x-ray sensitive photoconductor (direct detection). Since these devices are pixel arrays, the pixel size places an upper limit on the spatial resolution that can be achieved and is one of the fundamental design parameters of a detector. Many imaging applications are satisfied with a pixel size from 125 to $250 \mu\text{m}$ and such systems are in production.² However, it is desirable to achieve higher spatial resolution with pixel sizes in the range $50\text{--}100 \mu\text{m}$, and higher sensitivity.

High resolution sensors tend to have a reduced signal-to-noise ratio simply because of the small pixel size and a low fill factor. The fill factor, F , is defined as the fraction of the pixel area that is sensitive to incident radiation. A good approximation to the real situation is a square pixel of linear dimension, d_p , containing a contact electrode of dimension $a < d_p$, at which the charge generated by the sensor is collected. Processing considerations limit $d_p - a$ to $10\text{--}15 \mu\text{m}$ for typical arrays. Assuming an x-ray flux, q_0 , onto the surface, the charge, Q_C , developed at the pixel is

$$Q_C = q_0 \alpha_x G_x d_p^2 F, \quad (1)$$

where α_x is the fraction of the x rays absorbed, and G_x is the gain, defined as the charge detected per absorbed x ray. The fill factor has limiting values of

$$a^2/d_p^2 \leq F \leq 1. \quad (2)$$

The lower value assumes that the pixel is only sensitive to the x-ray flux above the collection electrode, while $F=1$ when the pixel is sensitive to the flux over its whole area. Small pixels therefore have an intrinsically reduced signal due to the $d_p^2 F$ term in Eq. (1). High resolution arrays therefore need sensors with high sensitivity for optimum performance, and this is achieved by a combination of high x-ray absorption, high gain, and high fill factor.

There are a number of possible approaches to achieve improvements in sensitivity. High fill factor designs for $a\text{-Si:H } p\text{-i-n}$ photodiode arrays give a substantial increase in sensitivity of indirect detection arrays, and when coupled to CsI phosphors yield high gain and high resolution. The characterization of detectors of this design, fabricated with a pixel size of $75 \mu\text{m}$ is reported elsewhere.^{3,4} Direct detection arrays usually give high resolution because they do not exhibit the image spreading effects characteristic of phosphors. Detectors based on selenium are successful,⁵ but still have some performance limitations, since the gain is less than might be expected, with the energy loss to produce a de-

^{a)}Electronic mail: street@parc.com

^{b)}Permanent address: Department of Physics, University of Stockholm, Sweden.

tected electron–hole pair being about 50 eV.⁶ Furthermore, even though the selenium is deposited as a continuous film, charge collection only occurs over the contact pads so that the signal is reduced by the fill factor according to the lower limit in Eq. (2).⁶ Selenium also has rather low x-ray absorption so that thick films and consequently high voltages are required for its operation.

This article describes measurements of high resolution image sensors using HgI₂ and PbI₂ in the direct detection mode of operation. We have explored these two rather similar materials as alternative x-ray photoconductors to selenium to determine if they can give better performance. Direct detector materials must have several attributes, including high charge collection, high x-ray absorption, low dark current, good uniformity, etc, and these are difficult to achieve in a single material. The focus of these studies is on the x-ray response in terms of sensitivity, spatial resolution, and other factors that are important to achieve a high detective quantum efficiency (DQE).

II. THE IMAGE SENSOR AND MEASUREMENT SYSTEM

The measurements are performed on 512×512 pixel arrays with 100 μm pixel size, using a fabrication process that is scalable to the large areas required for medical imaging. The pixel design is typical for direct detection devices, and is described elsewhere.⁷ The source of the amorphous silicon thin film transistor (TFT) is connected to the contact electrode, which is isolated from the rest of the pixel by an insulation layer, and the TFT gate and drain are connected to address lines for readout. The contact is almost square, with a minimum separation to the neighboring pads of 15 μm, and has a geometrical fill factor of 67% (note that an earlier publication incorrectly stated a high fill factor⁷). The pixel also contains a ~0.4 pF storage capacitor since the capacitance of the sensor film is insufficient by itself.

The array is addressed by an external shift register and charge is transferred to external amplifiers.¹ Typical operating conditions turn on the TFT gate for 20–30 μs, which is nearly 10 times the RC time constant of the TFT resistance and pixel capacitance. Correlated double sampling is used and the signal is digitized to 14 bits. Digital data is transferred to the host computer on a fiber-optic link, and the timing is performed by logic that can be programmed directly from the host. Electronic noise is <1000 electrons, without correction for line correlated noise which is smaller in magnitude than the random noise from the amplifiers. The response of the electronics is measured by injecting a calibration voltage pulse into a known capacitance at the input of the amplifiers.

A. HgI₂ and PbI₂ photoconductors

The PbI₂ films are deposited by thermal evaporation at a temperature below 200 °C, as described elsewhere.⁸ These are polycrystalline films with grain size of about 1–3 μm. The top electrode is a thermally evaporated Pd film, which is contacted by a single wire to provide the bias voltage. Several arrays with PbI₂ thickness from 60–240 μm have been studied. We have also studied companion PbI₂ films depos-

ited onto glass substrates, and some transport properties are reported elsewhere.⁹ Variations in the deposition conditions, particularly temperature, are found to give moderate changes in the sensitivity of the films.

The HgI₂ films are deposited by either thermal evaporation or by screen printing, using a slurry of HgI₂ crystallites in a polymer.^{10,11} In either case the active matrix substrate is coated with a layer of Humiseal to prevent chemical reactions with the underlying metals and to provide a blocking layer. Sample thickness varies from 80 to 250 μm, and the crystallite grain size is controlled by the deposition conditions and varies from 20 to 60 μm, estimated by visual inspection. Early samples of HgI₂ showed a very large variation in the response from pixel to pixel. Previously, we speculated that this was because of the large grain size, which was similar to the dimensions of the pixels.¹² Recent material with grain size at the low end of the range gave much better uniformity, seeming to confirm the trend with grain size. For the detailed investigation of sensitivity in Sec. IV B, we studied a sample of this type.

B. Measurement techniques

X-ray measurements are obtained with a dental x-ray generator that operates between 50 and 100 kVp, or with a mammography unit operating from 24 to 40 kVp. The dose is measured with a commercial dosimeter. Under normal usage, the array is readout continuously with a constant frame time selected by the operator that can be as small as 55 ms but is more typically 0.2–0.5 s. Measurements are generally made with a single exposure (i.e., the radiographic mode). Image lag measurements are made by recording the signal at a predetermined number of frames after the single exposure frame. The incident photon spectrum is obtained from published spectra for the two types of generator, including the additional filtering where appropriate, and is used to calculate the x-ray absorption, the photon flux, and the average energy.

To obtain the spatial resolution we use the angled slit technique,¹³ from which the line-spread function (LSF) is obtained directly and the presampled modulation transfer function (MTF) is its Fourier transform. We use a slit of 16 μm, which is small enough to prevent excessive broadening of the LSF, while allowing a sufficient signal for the measurement.

The image of the angled slit also provides a measurement of the relative sensitivity across the pixel, which gives information about the effective fill factor. The two-dimensional slit image is represented as $S(n_x, n_y)$, where n_x and n_y index the pixels in the x and y axes. The signal is summed in the direction perpendicular to the axis to which the slit is placed at the small angle, θ , to give

$$I(n_y) = \sum_{n_x} S(n_x, n_y). \quad (3)$$

At each value of n_y the slit is located in a different x -axis position on the pixel given with respect to a suitably chosen origin by

$$x = d_p \text{ modulus}(n_y \sin \theta), \quad (4)$$

so that $I(n_y)$ is transformed into $I(x)$, in the same way as is done to obtain the LSF. $I(x)$ plots the relative sensitivity as a function of position, and we usually plot this from the center of one pixel to the center of the next.

Many of the measurements reported below are of the signal as a function of bias voltage. The expected charge collection as a function of the bias is given in terms of the mobility-lifetime product ($\mu\tau$), by the Hecht formula,

$$\frac{Q}{Q_0} = \frac{\mu\tau E}{d} (1 - \exp[-d/\mu\tau E]) \equiv H(d, E), \quad (5)$$

where E is the applied field, d is the thickness, and Q_0 is the total charge.

The Hecht formula applies to electrons or holes created at one side of the sample, which drift to the other under a uniform applied field, $E = V/d$. The assumption of a uniform field is discussed later, in Sec. IV B. The formula is also based on the assumption that charge is created at the contact, so that only a single carrier type contributes to the signal. In our case, x-ray absorption always occurs over a significant fraction of the film thickness, and this can be analyzed by a generalization of Eq. (5). If a carrier is created at depth x , and drifts to the other side of the layer, then the charge collection follows the Hecht formula, $H(d-x, E)$, for the smaller distance $d-x$. The total charge collection is further modified by a multiplying factor that depends on the magnitude of $\mu\tau E/d$. The factor is $(d-x)/d$ if most of the charge is collected and unity if charge collection is small. The combined charge collection for both electrons and holes, and for an absorption distribution of $\alpha(x)$, for the case when most charge is collected, is therefore given by¹⁴

$$\frac{Q}{Q_0} = \frac{1}{d} \int_0^d dx \alpha(x) [(d-x)H_A(d-x, E) + xH_B(x, E)], \quad (6)$$

where the first term is the contribution from carrier A moving away from the absorbed x rays, and the second is from carrier B moving in the opposite direction. $H(x, E)$ is defined in Eq. (5) and $\alpha(x)$ can be calculated from the x-ray spectra and the material properties. It is easy to see that if $d\alpha/dx$ only has values very close to $x=0$, then the second term vanishes and the first term reduces to Eq. (5).

There are some useful approximations to Eq. (6) for three cases of interest. The first case assumes that only one carrier has a significant $\mu\tau$, but that the charge collection is reduced by a finite (but small) absorption depth. The charge collection then approximates to

$$\begin{aligned} \frac{Q}{Q_0} &\equiv H_A(d, E) \left[1 - \frac{1}{d} \int_0^d dx \alpha(x) x \right] \\ &= H_A(d, E) [1 - L(E_x)/d], \end{aligned} \quad (7)$$

where $L(E_x)$ is defined by the integral and its dependence on the x-ray energy, E_x , is made explicit. The term in brackets provides a correction factor to the measured collection.

The second case of interest is when the bias polarity is chosen to collect the carrier with the smaller $\mu\tau$, but the finite absorption depth provides some contribution of the larger $\mu\tau$ carrier moving in the reverse direction. The charge collection then approximates to

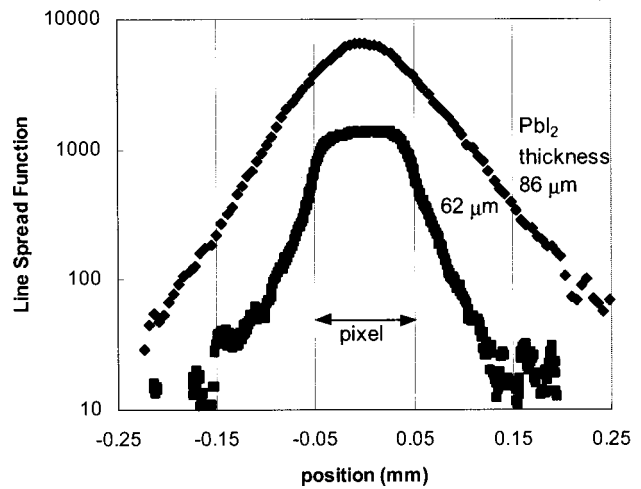


FIG. 1. The line-spread function data for two arrays with PbI_2 layer thickness of 62 and 85 μm , showing the additional broadening in thicker films. The vertical lines indicate the pixel boundaries.

$$\frac{Q}{Q_0} = H_A(d, E) + \frac{L(E_x)}{d}, \quad (8)$$

where it is assumed that all of the high $\mu\tau$ carriers are collected, and this provides a constant offset to the charge collection for the low $\mu\tau$ carrier.

The third case is for weakly absorbed x rays and single carrier collection, for which

$$\frac{Q}{Q_0} \equiv c\alpha(d), \quad 1 > c > 0.5. \quad (9)$$

In the limit of uniform absorption, the charge collection is just half the fraction of x-rays absorbed.

III. EXPERIMENTAL RESULTS

About ten arrays each of HgI_2 and PbI_2 have been studied. For each material, the arrays yielded results that are qualitatively similar but quantitatively depend on the specific sample, particularly as regards dark current and charge collection. A significant source of the differences is the grain size, but we do not yet have a complete understanding of the role of grain size. The results presented should be considered as representing the present state-of-the-art, rather than definitive values for the material, since further exploration of the deposition conditions and material composition might give improved properties.

A. Spatial resolution

Figure 1 shows the line spread function obtained using the angled slit technique for two PbI_2 arrays. The array with 62 μm PbI_2 has about 80% of the LSF confined to the central pixel. The additional broadening to the LSF decreases approximately exponentially into the adjacent pixels. The sharp drop in the LSF occurs near the boundary of the pixel rather than at the edge of the contact pad, thus indicating that charge is collected from almost the entire pixel and not merely over the contact pads, further data about the effective fill factor is given below. The LSF for the thicker 86 μm PbI_2

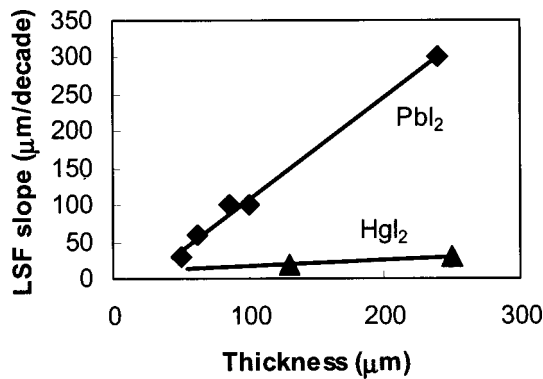


FIG. 2. Plot of the broadening of the LSF as a function of the film thickness for PbI_2 and HgI_2 . The broadening is the exponential slope of the LSF tails.

layer is significantly broader, extending further into the neighboring pixel. The LSF for a 240 μm thick film is observed to be much broader still. Further LSF data for 50 and 100 μm layers are published elsewhere,¹² and these compare measurements at high and low exposure energy (30–35 kVp versus 80 kVp). Virtually no dependence on the x-ray energy is observed. Figure 2 plots the slope of the LSF tail versus the sample thickness for the various samples measured and shows that there is an approximately linear increase in the LSF width.

Figure 3 shows the LSF for a 130 μm HgI_2 array measured at 50 and 60 kVp exposure. The LSF drops sharply at the edge of the pixel and the tail is consistent with the width of the measurement slit, so that there is virtually no image spreading. The residual signal at the 1% level is probably due to effects arising from the readout electronics. An LSF measurement for a 250 μm thick film also showed little image spreading, although the nonuniformity of the sensitivity reduced the quality of the data.¹² HgI_2 and PbI_2 therefore exhibit quite different LSF behavior with increasing film thickness, as shown by the comparison in Fig. 2.

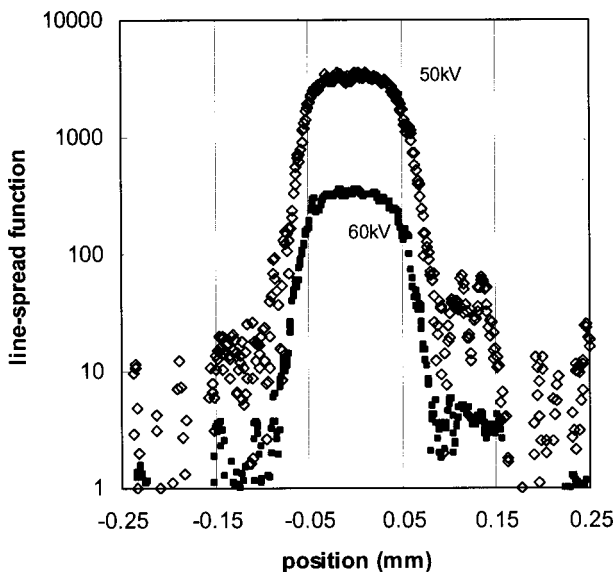


FIG. 3. The line-spread function data for an array with 130 μm of HgI_2 , showing little broadening. The vertical lines indicate the pixel boundaries.

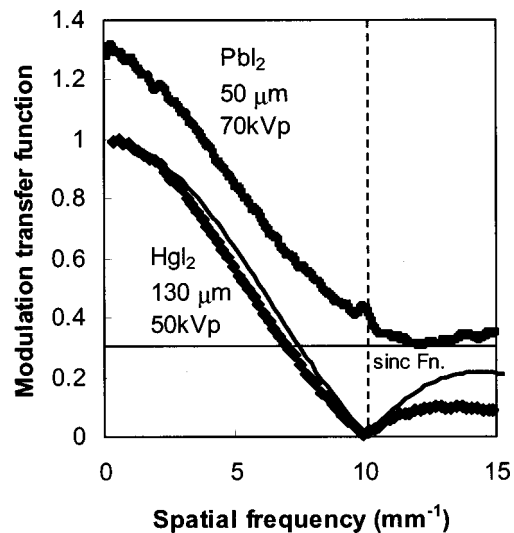


FIG. 4. Modulation transfer function data for PbI_2 and HgI_2 , and a comparison with the sinc function. Note that the first minimum for PbI_2 is beyond the spatial frequency of the pixel array (indicated by the vertical line). The PbI_2 data is shifted vertically by 0.3 for ease of viewing.

When the LSF exhibits only small broadening, the MTF approximates to the form expected for an ideally abrupt LSF, which is $\text{sinc}(\pi u d)$, where u is the spatial frequency. Figure 4 shows a comparison of the MTF of HgI_2 and a thin PbI_2 film. The differences in the shape reflect the broadening of the LSF and the degree of sensitivity in the gap between pixels, as discussed in Sec. III C. Thicker PbI_2 films have a reduced MTF because of the increasing width of the LSF.

In a previous publication we suggested that the spread of the LSF in PbI_2 may be due to x-ray fluorescence at the iodine K -edge located at 33 keV.⁷ The supposition was that fluorescent x-rays would travel laterally and be reabsorbed, thus broadening the LSF. The LSF data now shows that this explanation cannot be the major effect, although fluorescence broadening presumably exists at some smaller level. The evidence that k -fluorescence plays no major role is that, (1) the LSF is virtually identical for exposure above or below the 33 keV iodine edge,¹² and (2) the broadening effect with increasing thickness is not seen in HgI_2 , which should be essentially identical to PbI_2 as regards x-ray fluorescence. The additional broadening of the LSF in PbI_2 that is not observed in HgI_2 indicates that some fundamentally different mechanisms are occurring in the two materials. The origin of the PbI_2 broadening is discussed in Sec. IV C.

B. Charge collection and bias dependence

Figure 5 shows the signal versus bias for the 130 μm HgI_2 array, applying negative bias to the array and showing measurements at 80 and 24 kVp exposure. The form of the data for other arrays is the same, with the signal increasing with bias and eventually approaching saturation. The lines in Fig. 5 show fits to Eq. (5) and give essentially the same $\mu\tau$ value of $\sim 1.5 \times 10^{-5} \text{ cm}^2/\text{V}$ for the two measurements. We have studied several HgI_2 films and find that $\mu\tau$ for electrons are in the range 6×10^{-6} to $6 \times 10^{-5} \text{ cm}^2/\text{V}$.¹² These samples cover a range of crystallite size and include both

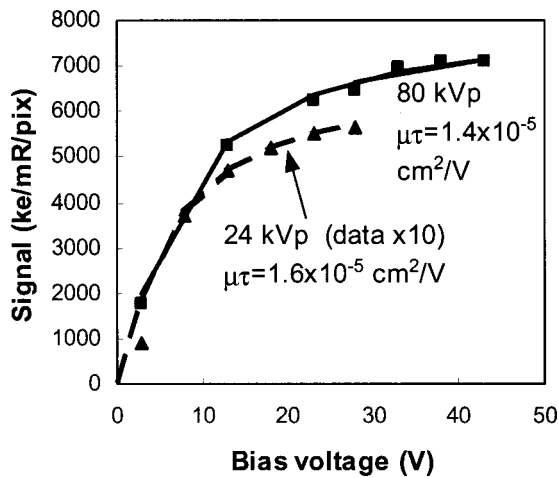


FIG. 5. Electron charge collection for HgI₂ measured at 24 and 80 kVp exposure. The lines indicate the fit to Eq. (5) with the $\mu\tau$ values as indicated.

evaporated and screen printed material. Figure 6 shows how the measured electron $\mu\tau$ values vary with crystallite size. Although there are substantial variations, it seems that large crystals give high values of $\mu\tau$, at least for the evaporated material. The dependence on crystal size is less clear for the screen printed material, but since the $\mu\tau$ values are lower, another mechanism might mask the crystal size dependence.

The initial distribution of carriers depends on the x-ray energy. Only for the low energies (i.e., 24 kVp) is the absorption very close to the top contact and in this case we can be sure that the carriers being collected are electrons, and that holes contribute little to the signal. For high energy exposure, the absorption is more uniform through the sample, and there may be contributions from both signs of carriers.

Figure 7 shows the charge collection under both bias polarities for a screen printed sample of HgI₂ and at low energy exposure. The sample of Fig. 5 did not sustain a large enough positive bias to get good data, but the low field results are generally similar, and the same behavior is also found in the other samples. The charge collection of holes is evidently much smaller than that of electrons. The hole charge collection increases slowly with bias after an initial jump at the lowest bias voltage. We interpret this as a mixed contribution from both electrons and holes, due to the finite absorption depth of the x rays. Figure 7 includes the fit to Eq.

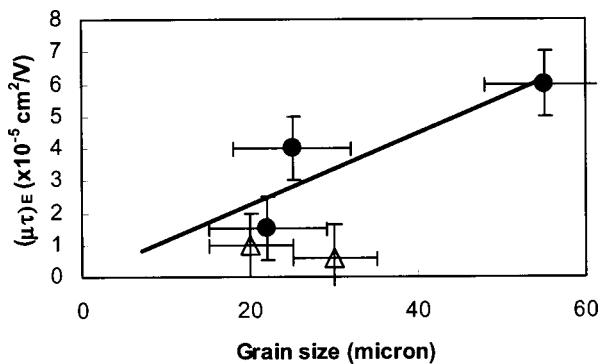


FIG. 6. Plot of the dependence of the electron $\mu\tau$ values on crystallite size for both evaporated and screen printed samples.

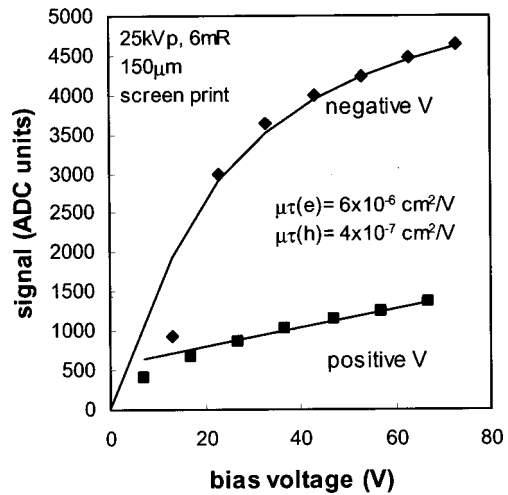


FIG. 7. Electron (negative V) and hole (positive V) charge collection for a screen-printed HgI₂ array measured at 25 kVp exposure. The lines indicate the fit to Eq. (5) for electrons and Eq. (8) for holes, with the $\mu\tau$ values as indicated.

(8) for the hole response, with the electron collection amounting to ~ 0.04 . This implies an average absorption depth, $L(E_x)$ of 10 μm , and calculations show that 40% of the x rays are absorbed within 10 μm , which is reasonably consistent. The fit to the data shows that the $\mu\tau$ product for holes is about 15 times less than for electrons which implies that holes contribute little to the signal. The $\mu\tau$ value for holes is measured to be $(4 \text{ to } 5) \times 10^{-7} \text{ cm}^2/\text{V}$ for all the samples measured, so the ratio of electron and hole $\mu\tau$ reaches ~ 100 in the evaporated samples with large grain size. Hence for the HgI₂ films measured, the electron charge collection is always larger than the hole collection. The hole $\mu\tau$ shows no obvious correlation with the material structure, but this is a difficult value to obtain accurately because the charge collection is so small.

Similar measurements of charge collection have been made for PbI₂ films, and one example is shown in Fig. 8 for 25 kVp excitation, and others are reported elsewhere.^{7,12} In this case the hole collection exceeds the electron collection,

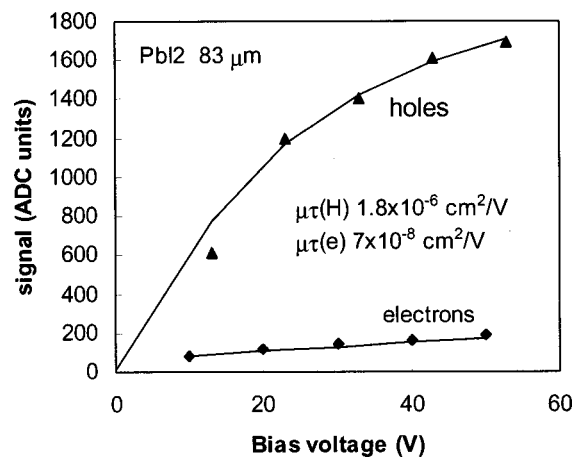


FIG. 8. Hole and electron charge collection for a PbI₂ array showing the fits to Eqs. (5) and (8) and the deduced $\mu\tau$ values for holes and electrons.

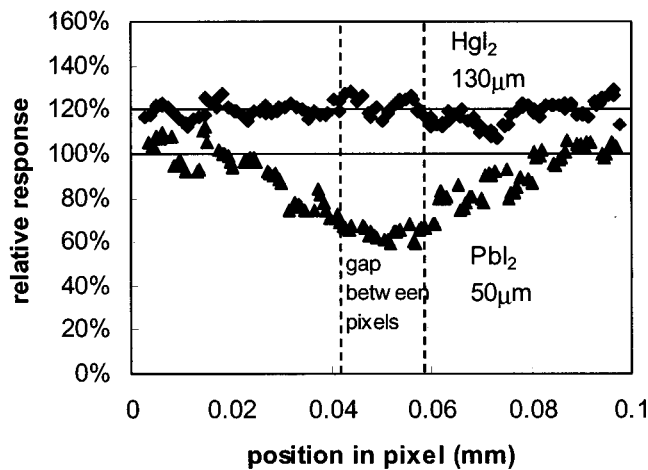


FIG. 9. Position dependence of the PbI_2 and HgI_2 charge collection in the region between two contact pads on adjacent pixels, obtained from the angled slit data. The gap between pixels is indicated by the dashed line. The HgI_2 data are shifted vertically by 20% for ease of viewing.

which is opposite to HgI_2 . The fit of Eqs. (5) and (8) to the data gives values of $1.8 \times 10^{-6} \text{ cm}^2/\text{V}$ for holes and $8 \times 10^{-8} \text{ cm}^2/\text{V}$ for electrons, which are smaller by a factor of 3 or more compared to the pairs of values obtained for HgI_2 . Since the crystallite size for PbI_2 is smaller than for HgI_2 , perhaps the charge collection data are described by the same trend as shown in Fig. 6. However, as discussed in Sec. IV B, there is reason to doubt the validity of the simple charge collection fit to the data, so these values should be treated as tentative.

C. Charge collection in the pixel gap

The evaluation of the sensitivity also requires a knowledge of the effective fill factor, as described in Eq. (1). The angled slit image data is used to find the sensitivity as a function of position within the pixel, and this data is shown for both PbI_2 and HgI_2 in Fig. 9 using the technique described in Sec. II B. The measurements find a decrease in the sensitivity of the PbI_2 array for illumination above the gap. The decrease is to about 60% of the signal over the contact pad, and on a different sample the reduction was to 80%.⁷ Since the slit width is as wide as the gap, the actual response of the array would require a deconvolution of the slit width

from the measured response. While a precise deconvolution is not possible with the present data, it is evident that the average response from within the slit region is $\sim 50\%$ of the response from directly over a PbI_2 contact. On the other hand the data for HgI_2 shows no drop in sensitivity in the gap between pixels, with a detection uncertainty of about 5%. Similar measurements using a selenium photoconductor find a larger loss of charge between the pads, consistent with the LSF observations made by others.⁶

When the two dimensions of the contact are considered, the effective fill factor for charge collection in the PbI_2 array is estimated to be about 85% ($\approx 0.67 + 0.5 \times 0.33$). The drop in sensitivity in the gap for PbI_2 is also evident in the MTF data of Fig. 4. The first minimum in the MTF occurs at the inverse of the effective sensitive size of the pixel. The pixel size is 0.1 mm, so that the minimum should occur at 10 mm^{-1} if the pixel is fully sensitive. For the PbI_2 data, the minimum actually occurs at $\sim 11 \text{ mm}^{-1}$, indicating a slightly smaller effective pixel size, while for HgI_2 the MTF minimum is at 10 mm^{-1} .

D. Image lag

Image lag also provides a mechanism for loss of sensitivity which needs to be quantified. Figure 10 compares the image lag of PbI_2 and HgI_2 under comparable excitation conditions and with the bias polarity that favors high charge collection. The lag is very different for the two materials. The HgI_2 data are typical of other materials with a lag after the first frame of $\sim 10\%$, and while the subsequent frames decrease less slowly, the lag quickly drops to below 1%. The integrated total signal in the lag frames is estimated to be $\sim 20\%$ of the signal in the first frame. In contrast, the image lag of PbI_2 decreases much more slowly, with about 30% in the first frame and still $>10\%$ after ten frames. In this case the total signal in the lag frames exceeds the signal in the first frame by a wide margin, which is about a factor of 5.

E. Dark current and dark noise

Both HgI_2 and PbI_2 have significant dark leakage current, which varies widely for different arrays. Dark current can limit the utility of the material for x-ray detection, since it prevents application of a sufficiently high field to optimize the charge collection. The typical leakage current of PbI_2 arrays studied so far is in the range $10\text{--}50 \text{ pA}/\text{cm}^2$ at a bias

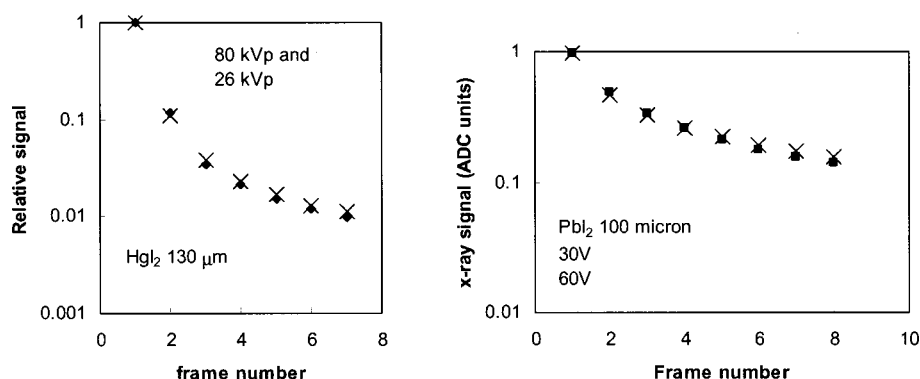


FIG. 10. Image lag data for HgI_2 and PbI_2 , showing the much larger lag for PbI_2 . The lag shows little dependence on excitation energy or bias voltage.

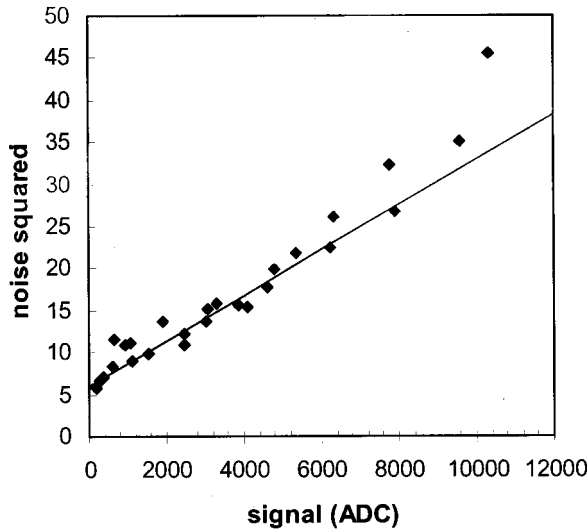


FIG. 11. The mean square dark noise plotted vs dark signal in ADC units for a 62 μm thick PbI_2 layer. The solid line is the predicted fit assuming shot noise.

of 1 $\text{V}/\mu\text{m}$, which is within the range of currents measured on test samples of PbI_2 . The range for HgI_2 is 8–10 pA/mm^2 at 1 $\text{V}/\mu\text{m}$ for screen printed and 10–50 pA/mm^2 at 0.2 $\text{V}/\mu\text{m}$ for evaporated films.

In the presence of a significant dark current, it is important to understand its noise contribution. An example of the dark signal noise for a 62 μm thick film of PbI_2 is shown in Fig. 11. The rms values are obtained from successive image frames and are obtained as an average over at least 3000 pixels. The total dark signal charge, Q_D , is

$$Q_D = I_D(V)t_F, \tag{10}$$

where t_F is the imager frame time and $I_D(V)$ is the voltage-dependent dark current. The measurements varied the bias from 0 to 40 V and t_F from 0.055 to 3 s. After changing the bias, the current drifts significantly, as observed earlier,⁹ and was allowed to settle for some minutes before the measurement started.

Ideal shot noise from the detector leakage current would result in a measured noise given by

$$n_m^2 = Q_D/e + n_{\text{add}}^2 \quad (\text{electrons}), \tag{11}$$

where n_{add}^2 is the additive rms noise from the readout electronics and e is the electronic charge. When the signals are measured in ADC units, the relation includes the system calibration constant, g_{sys} (electrons/ADC),

$$n_m^2 = Q_D/eg_{\text{sys}} + n_{\text{add}}^2 \quad (\text{ADC units}). \tag{12}$$

The solid line in Fig. 11 corresponds to the measured calibration of the system (in this case 372 e/ADC), and provides a good fit to most of the noise data. We can infer the following from the measurements.

(1) For most measurement conditions, the dark current noise is explained by the theoretically predicted shot noise. A small amount of excess noise seems to be present at high bias and with long integration times. Its origin is unclear but is probably due to drift in the leakage current.

(2) The fit to the system calibration provides an independent verification that the calibration of the system response is accurate. This is a valuable result since the calibration depends on the capacitor used to inject charge into the amplifier which is calculated from the chip design, rather than measured.

(3) The additive noise of the electronic system is the extrapolation of the noise data to zero bias, and gives an rms value of 800–900 electrons, which is consistent with the expected performance of the readout amplifier. No correction is made for line noise in these measurements.

The distribution of leakage current across the array has been measured for the same PbI_2 film. Over most of the area, the dark current is uniform within a standard deviation of $\sim 5\%$ of the dark signal, as measured by a histogram of pixel values. The uniformity decreases slightly as the bias is increased. There are, in addition, some areas of the array, usually roughly circular with diameter ~ 0.5 mm, that have a much higher leakage current, due to some unknown defect in the PbI_2 film.

IV. DISCUSSION

The discussion focuses on three main issues resulting from the comparison of HgI_2 and PbI_2 data. First is to establish whether the sensitivity can be explained in terms of the expected ionization and charge collection processes. Second is to identify what are the material differences that cause PbI_2 and HgI_2 to respond differently. Third is to understand why the LSF of PbI_2 broadens in thick films, but does not in HgI_2 .

A. The x-ray sensitivity of HgI_2 and PbI_2

The main issue from the sensitivity data is whether we can fully account for the measured signal. The HgI_2 case is less complicated than PbI_2 and this is considered first. It is helpful to calculate an effective ionization energy, W_{eff} , which is defined from the measured gain described in Eq. (1), by

$$W_{\text{eff}} = \beta E_{x\text{av}}/G_x \quad (\text{eV}) \tag{13}$$

where $E_{x\text{av}}$ is the average x-ray photon energy and $\beta (< 1)$ is a product of factors representing corrections to the signal from various loss mechanisms that reduce the gain. Provided all the losses are understood, W_{eff} should equal the internal ionization energy, W , which for both HgI_2 and PbI_2 is about 5 eV.^{8,10} A comparison of W_{eff} with W is therefore a convenient metric to compare the x-ray sensitivity with the theoretical value. The correction factor can be written as a product of the terms,

$$\beta = \beta_{\text{abs}}\beta_Q\beta_{\text{gap}}\beta_{\text{lag}}, \tag{14}$$

where the loss factors are from incomplete x-ray absorption (β_{abs}), incomplete charge collection (β_Q), incomplete charge collection in the gap between pixels (β_{gap}), and image lag (β_{lag}),

We first consider measurements at low energy exposures. The raw data for the 130 μm HgI_2 array in Fig. 5 gives a sensitivity of 566 ke/mR/pixel at 25 kVp and a bias of 28 V. We calculate the photon flux (298 ph/mR/pixel) and the average energy (15.2 eV) to obtain W_{eff} (with $\beta = 1$) of 7.8 eV,

TABLE I. Measured sensitivity of HgI₂ and PbI₂ and the various correction factors used to obtain the corrected value of W_{eff} .

	HgI ₂ 25 kVp	HgI ₂ 80 kVp	PbI ₂ 30 kVp	PbI ₂ 80 kVp
measured W_{eff}	7.8	19.6	36	180
correction for absorption	1.0	0.49	0.98	0.51
correction for charge collection	0.77	0.65	0.78	0.4
correction for pixel gap	1.0	1.0	0.85	0.85
correction for lag	0.82	0.82	~0.2	~0.2
corrected W_{eff}	4.9	5.1	5	6

as indicated in Table I. For these low energy x-rays, the absorption is essentially complete. The charge collection correction contains three components. One is the incomplete collection of electrons at the specific bias voltage, and we use the Hecht formula fit to obtain the correction factor of 0.81. The second correction is the absorption depth that implies that full collection of electrons does not yield the full charge [see Eq. (7)], and this factor is calculated to be 0.83. Third is the small collection of holes, which partially offsets the second factor. Taken together we estimate $\beta_Q = 0.77$. The losses in the gap between pixels are negligible from Fig. 9, and the lag factor is measured to be 0.82. Combining these factors gives a corrected W_{eff} of ~ 5 eV (see Table I).

The calculation is repeated for exposure to high energy x-rays, for which the corrections for absorption and the charge collection of a single carrier are more significant, so that the uncorrected value of W_{eff} is 19.6 eV at an exposure energy of 80 kVp. The individual correction estimates are again shown in Table I obtained in the same way as for the low energy exposure and result in a slightly higher value of W_{eff} but consistent within the uncertainty in the estimates. The measured W_{eff} is shown in Fig. 12 as a function of exposure energy, and the W_{eff} values calculated after the correction for x-ray absorption are also shown to illustrate that they are almost independent of energy.

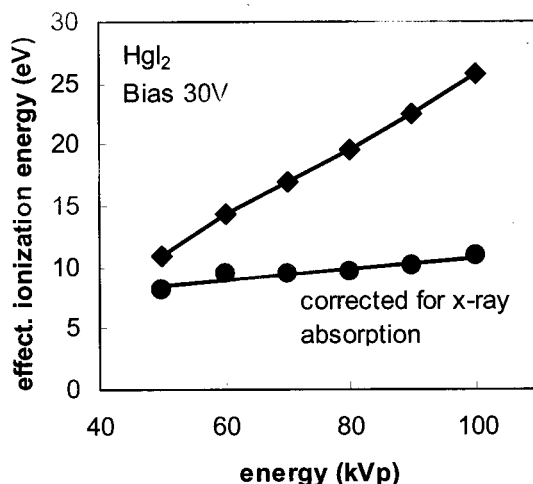


FIG. 12. The effective ionization energy, W_{eff} for 130 μm thick HgI₂ measured as a function of the exposure energy and with the array biased for electron collection. Also shown is W_{eff} after the calculated correction for x-ray absorption, which is the major loss factor in this energy range.

As a result of this analysis, the measured W_{eff} is ~ 5.0 eV after all losses have been corrected, and agrees with the known internal ionization energy within the measurement uncertainty. Hence we conclude that all the losses have been identified and estimated with reasonable accuracy.

There are, however, some unresolved questions that could affect the calculations. The losses attributed to charge collection and image lag might be double-counting the same effects, since charge that is trapped and undetected in the first frame might be released later and contribute to image lag. In particular, it would be valuable to understand better the transport of the holes, which we know are collected very inefficiently. The hole contribution to the lag signal should be much larger for high energy exposure because of the deeper absorption depth. However, the image lag is observed to be independent of exposure energy suggesting that holes do not contribute to the lag. If holes are not detected in the image lag data, then an unresolved question remains whether they are swept out more slowly, remain trapped, or recombine with electrons.

The equivalent values of W_{eff} for PbI₂ are also shown in Table I for an 83 μm thick sample, using the same procedure. The initial measured values are far higher than for HgI₂ by factors of 4–8, and in other samples W_{eff} is even larger.¹² Part of the difference can be attributed to the loss factors associated with the absorption and charge collection, but by far the dominant correction factor is the image lag. This correction is by a factor of 5, compared to about 20% for HgI₂. Once the large image lag is included, however, the corrected W_{eff} approaches the theoretical value of W , although the uncertainty in the lag correction is large.

This comparison shows that the two striking differences between the x-ray response of PbI₂ compared to HgI₂ are the large image lag and the extra width of the LSF. The next sections discuss material properties and a proposal for the origin of these differences.

B. Materials differences between HgI₂ and PbI₂

Given that the two materials are so similar, it is notable that the primary charge detected is opposite, electrons in HgI₂ and holes in PbI₂. However, we also know that the transport type is opposite, with HgI₂ being n type and PbI₂ being p type.^{9,10} In either case the Fermi energy is quite deep (0.7 to 0.8 eV) to account for the low conductivity, compared to the band gap of 2.0–2.5 eV. It is not difficult to understand how the observed charge collection properties can occur. The

$\mu\tau$ value reflects the trapping of carriers by deep states in the band gap. We suppose that there is some distribution of localized trapping states within the gap that is generically similar in the two materials. An n -type material (i.e., HgI₂) has its Fermi energy largely above the defect states, so that most defects are fully occupied by electrons and will therefore trap holes more efficiently than electrons. The opposite applies to a p -type material, for which the same defects will primarily act as electron traps. Neither material is deliberately doped, so the different conduction type is presumably the result of inadvertent dopants introduced in the starting material or by the deposition process.

In the absence of specific knowledge about the defects in these materials we can only give broad estimates of the defect densities. Assuming typical capture cross sections, σ , of 10^{-15} cm², a thermal velocity, v , of 10^7 cm/s, and an estimated carrier mobility of 10 cm²/V s,¹⁰ the usual formula for the carrier lifetime ($\tau = 1/N\sigma v$) allows us to relate the $\mu\tau$ value to a trap density. A $\mu\tau$ value of 10^{-5} cm²/V, as in high quality HgI₂ films, corresponds to about 10^{13} cm⁻³ electron traps. There should be about 50 times more hole traps in PbI₂, and in each case the minority carrier apparently sees 10–100 times more defects than the majority carrier. With these values, it only takes a 10^{15} to 10^{16} cm⁻³ concentration of inadvertent dopants to move the Fermi energy. The results in Fig. 5 indicate a correlation between $\mu\tau$ and the grain size, suggesting that the traps are grain boundary defects, which is a reasonable expectation for polycrystalline films. The good quality HgI₂ has a grain size of 30–60 μ m, for which we estimate a density of surface atoms of $\sim 10^{18}$ cm⁻³. That this density of surface atoms results in 10^{15} cm⁻³ minority carrier defects seems reasonable, and perhaps indicates that the grain boundary surfaces are rather inactive. The grain size is smaller in PbI₂ than HgI₂, and perhaps explains the smaller values of $\mu\tau$.

The charge collection is modeled in terms of Eq. (5), which assumes a uniform electric field in the sample. Given the estimates of the defect density we can ask whether this basic assumption is realistic. A conventional doped semiconductor with a blocking contact forms a depletion layer, beyond which is a field-free region. The depletion layer width is given by $[2\epsilon\epsilon_0 V/eN]^{1/2}$, for which a depletion layer of 100 μ m at a bias of 50 V requires a defect density of about 10^{13} cm⁻³. It seems marginally plausible that HgI₂ might be fully depleted but not PbI₂, with a higher defect density.

However, the physical situation is more complicated in low conductivity materials because the bulk conductivity can blur the distinction between the depletion layer and the undepleted part of the film. Any leakage current must pass through the undepleted region, which requires an electric field of J_L/σ_B , where J_L is the leakage current and σ_B is the bulk conductivity. When σ_B is small enough, the field in the undepleted region may be comparable to the depletion layer field. This situation is illustrated in Fig. 13, where we calculate the potential profile based on some simple assumptions. The depletion layer is defined by a single trap and chosen to be 30 μ m wide, and the applied voltage is split between the depletion layer and the voltage drop of the bulk resistance. The figure compares three conditions where the bulk conduc-

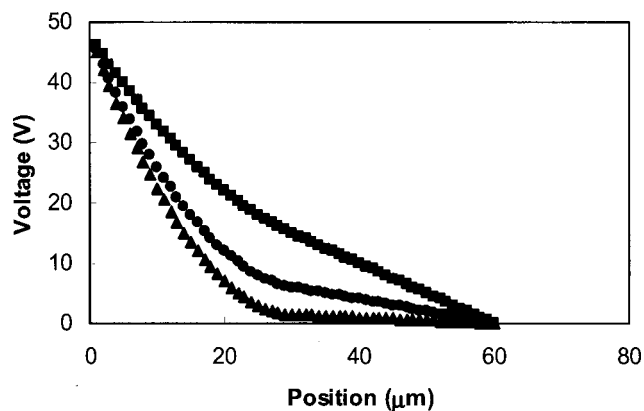


FIG. 13. Calculated potential profiles for the depletion layer model, for an assumed depletion layer width of 30 μ m, a leakage current of 5×10^{-9} A/cm², and bulk conductivity values of 10^{-12} , 2.5×10^{-12} , and 10^{-11} Ω^{-1} cm⁻¹.

tivity varies by a factor of 10 and illustrates that this is sufficient to determine whether the field is roughly uniform or whether there is region of low field. For an assumed leakage current of 5×10^{-9} A/cm², the corresponding bulk conductivity is 10^{-12} , 2.5×10^{-12} , and 10^{-11} Ω^{-1} cm⁻¹ for the three calculations in Fig. 13. Both the leakage and the conductivity are of the correct order of magnitude observed in PbI₂.

The point of this discussion is to propose that the different properties of the two materials relate to the internal field distribution. The HgI₂ sensitivity can be readily explained by the measured charge collection and some small loss corrections, and the Hecht model seems to give a good fit to the data, indicative of a more or less uniform internal field. We propose that the different properties of PbI₂ can be explained by a nonuniform internal field, as described next.

C. Depletion layer model for PbI₂ charge collection

The extremely large image lag is the key observation that supports the idea of an internal depletion layer in PbI₂. Charge collection in the depletion layer model consists of two processes. Carriers generated within the high field of the depletion layer are rapidly transported to the edge of the depletion layer. The charge is then transported more slowly by the bulk conductivity of the low field region. The effect on the charge collection can be described by a model in which the depletion layer is a capacitance, C_{depl} , and the field-free region is a series resistance, R_{bulk} , which is the standard description of a semiconductor depletion layer. This situation provides a model for the fast and slow charge collection process. The fast process corresponds to transport across the depletion layer and the fraction of the charge that is detected is roughly L_D/d , where L_D is the depletion layer width. The slow process occurs as the charge passes through the low field region, and takes the RC time constant of the depleted device.

It is known from studies of other sensor arrays that a series resistance does cause very large image lag, because the charge is collected with a long RC time constant. A recent study of color sensors found exactly this effect and a detailed

TABLE II. Calculation of W_{eff} based on the depletion layer model. The depletion layer width is assumed to be $30 \mu\text{m}$.

Exposure conditions	Response ke/mR/pixel	Calculated correction factor	W_{eff} (eV)
100 kVp; +ve	560	0.0229	6.3
100 kVp; -ve	360	0.0164	7.2

analysis of the relation between the series resistance and the image lag is given.¹⁵ Furthermore, other measurements have shown the nonuniform internal field that indicates the presence of a depletion layer in the PbI_2 layers. Time-of-flight transport studies of simple films found that the response is different if the measurement is performed promptly or a longer time after the voltage is applied.⁹ The electric field is uniform immediately after the voltage is applied, and the subsequent change in the transient current clearly showed a redistribution of the internal field. Related measurements also found a slow decay of the dark current over a long time, which is consistent with the emission of charge during the formation of a depletion layer.⁹

The PbI_2 image lag data in Fig. 10 show that after the first few frames, the signal decays with a time constant of about 2 s, which we associated with $R_{\text{bulk}}C_{\text{depl}}$. An estimated depletion layer width of $30 \mu\text{m}$ in the PbI_2 film has a capacitance of ~ 10 fF per pixel, and so a series resistance of order $2 \times 10^{14} \Omega$ gives the observed time constant. The corresponding resistivity is $\sim 3 \times 10^{12} \Omega \text{cm}$, which is consistent with previous measurements of the bulk conductivity.⁹

The x-ray sensitivity of PbI_2 was recalculated based on charge collection from a depletion layer width of $30 \mu\text{m}$, and the results are shown in Table II comparing positive and negative bias. The model assumes that the measurement only detects the fast collection across the depletion layer and that only holes contribute to the transport. The correction factor is based on the calculated x-ray absorption profile across the depletion layer for the specific measurement conditions. The correction is large but gives reasonable values for W_{eff} , which are also consistent for measurements made in either bias polarity. The same analysis was repeated for other x-ray conditions and gave similar results. These data show that the depletion layer model is in reasonable quantitative agreement with the data.

According to this model for the PbI_2 response, the generation of electron-hole pairs by ionization is efficient, with ionization energy close to the single crystal value of ~ 5 eV. The sensitivity is reduced by two primary factors. First, only holes are collected and electrons are trapped, and this reduced the signal by 20%–70% depending on the bias polarity and the x-ray energy. Second, when the sample is not fully depleted, only part of the signal is recorded in the first measurement frame and the remainder is detected very slowly. The second factor depends on the sample thickness.

The other interesting aspect of the proposed depletion layer model for PbI_2 is that it offers an explanation for the width of the LSF. When the carriers reach the field-free region, they move under the action of a low electric field. Rather than being directed vertically towards the contact

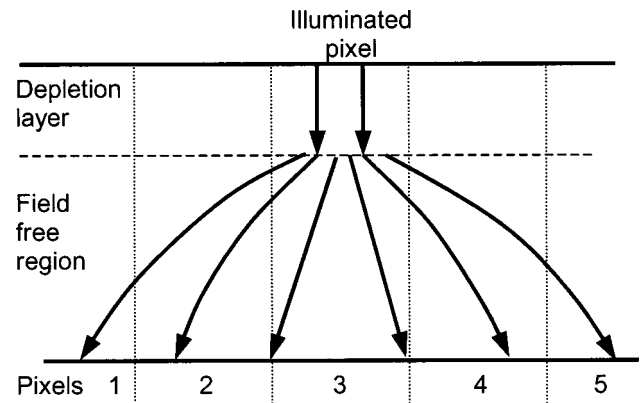


FIG. 14. Illustration of the lateral charge flow in the field-free region for the proposed depletion layer model.

electrode by the field, they will tend to spread out laterally, as illustrated in Fig. 14. Partly this lateral current flow is due to the natural spreading resistance of the field-free layer, but it may also be increased by the repulsive field of the charge that has accumulated at the illuminated pixel. The resulting image spread is expected to scale with the thickness of the field-free region. Hence no broadening of the LSF is expected for films up to the depletion layer width, and the broadening should increase as the films become thicker. Figure 2 shows that the increasing slope of the LSF wings in various PbI_2 films is consistent with this model and suggests that the depletion layer width is indeed roughly $30 \mu\text{m}$, as we have assumed.

D. The effect of material parameters on the DQE

The detective quantum efficiency (DQE) provides the generally accepted measure of image sensor performance. A detailed analysis of the DQE for the general type of large area pixel arrays has been given by Cunningham *et al.* and Siewedsen *et al.*^{16,17} An approximation to the zero frequency DQE, under conditions of negligible image spreading is

$$\text{DQE}(0) = \alpha_x F / [1 + \gamma + \sigma_{\text{add}}^2 / G_x Q_C], \quad (15)$$

where γ is the additional noise arising from the x-ray conversion process and Q_C is the signal charge, given by Eq. (1).

Measurements of x-ray sensitivity are key inputs to the DQE, but by no means the only factors. It is evident from the $\sigma_{\text{add}}^2 / G_x Q_C$ term in Eq. (15) that the effect of high sensitivity on the DQE depends on the magnitude of the additive noise and the exposure. It is well understood that in these flat panel systems, the DQE drops at low dose because of the additive noise, and that high sensitivity can extend the performance to lower doses.^{17,18}

Particularly in direct detection arrays, the fill factor F may influence the DQE independently of its effect on the signal, Q_C [see Eq. (1)]. There is a more direct effect on the DQE since the information contained in the undetected x-rays is lost, just as it is for nonabsorbed x-rays. The factor $\alpha_x F$ in the numerator of Eq. (15) reflects the loss of image information irrespective of the size of the signal and the additive noise. When interactions in the conversion layer cause

significant image spreading, then the factor F is not present in the numerator of Eq. (15), as is the situation for indirect detection with a phosphor. Thus HgI₂ shows a high fill factor and sharp LSF, while Se is reported to have a lower fill factor and also a sharp LSF, so that some loss of DQE results. PbI₂ has a lower fill factor than HgI₂ but also a broader LSF for the thicker films. Further studies are needed to determine how the proposed mechanism for the PbI₂ broadening affects the DQE.

The collection of charge in the gap between pixels is therefore significant for the performance of the image sensor. For our specific design parameters ($F=0.67$), the collection of charge created in the gap potentially enhances the DQE by 50% (i.e., by the factor $1/F$). The spatial resolution measurements show that a large fraction of this charge is indeed collected. It is interesting to note an apparent correlation between the $\mu\tau$ values and the collection in gap. The increase in effective fill factor going from Se to PbI₂ and to HgI₂ tracks the corresponding increase in $\mu\tau$ values for these three materials. It is easy to see that high $\mu\tau$ promotes charge collection by the smaller lateral collection fields in the gap between pixels.

V. SUMMARY

Polycrystalline PbI₂ and HgI₂ have been evaluated as new direct detection x-ray sensor materials, based on measurements with a complete α -Si:H matrix addressed image sensor system. The high sensitivity of HgI₂ films can be explained in terms of the theoretical ionization energy of about 5 eV, coupled with a set of mostly small correction terms arising from incomplete x-ray absorption, incomplete charge collection, and image lag. On the other hand, it is less easy to explain the sensitivity of PbI₂ films primarily because of the very large image lag that is observed. We propose a model to explain the difference in the response of the two materials based on the internal electric fields. While HgI₂ films have an approximately uniform internal field, PbI₂ films are more closely described by a depletion layer model. This model also accounts for the increase in the width of the line-spread function with thickness and is consistent with previous transport measurements.

ACKNOWLEDGMENTS

The authors are grateful to the members of the PARC process line for fabricating arrays, to P. Bennett for assis-

tance in the deposition of PbI₂ films, to B. Reisman and A. Zuck for assistance in the deposition of HgI₂ films, and to L. Antonuk and M. Scheiber for helpful discussions. This work is partially supported by NIST (70NANB7H3007), NIH (R01-CA56135 and R01-CA76405), and the NSF (DMI-9660842).

- ¹R. A. Street, *Technology and Applications of Amorphous Silicon*, edited by R. A. Street (Springer, New York, 1999), Chap. 4.
- ²See, for example, many publications in SPIE conference proceedings on The Physics of Medical Imaging, Proc. SPIE **3977** (2000) and **4320** (2001).
- ³J. T. Rahn, F. Lemmi, R. Weisfield, R. Lujan, P. Mei, J.-P. Lu, J. Ho, S. E. Ready, R. B. Apte, P. Nylén, J. B. Boyce, and R. Street, Proc. SPIE **3659**, 510 (1999).
- ⁴M. Mulato, S. Ready, K. Van Schuylenbergh, J. P. Lu, and R. A. Street, J. Appl. Phys. **89**, 8193 (2001).
- ⁵D. L. Lee, L. K. Cheung, B. Rodericks, and G. F. Powell, Proc. SPIE **3336**, 14 (1998).
- ⁶W. Zhou, I. Blevis, S. Germann, and J. A. Rowlands, Proc. SPIE **2708**, 523 (1996).
- ⁷R. Street, J. T. Rahn, S. E. Ready, K. Shah, P. R. Bennett, Y. Dmitriyev, P. Mei, J.-P. Lu, R. B. Apte, K. van Schuylenbergh, F. Lemmi, J. B. Boyce, and P. Nylén, Proc. SPIE **3659**, 36 (1999); R. Street, S. E. Ready, J. T. Rahn, M. Mulato, K. Shah, P. R. Bennett, P. Mei, J.-P. Lu, R. B. Apte, J. Ho, K. van Schuylenbergh, F. Lemmi, J. B. Boyce, P. Nylén, M. Scheiber, and H. Hermon, *ibid.* **3977**, 418 (2000).
- ⁸K. S. Shah, F. Olschner, L. P. Moy, P. Bennett, M. Misra, J. Zhang, M. R. Squillante, and J. C. Lund, Nucl. Instrum. Methods Phys. Res. A **380**, 266 (1996); K. S. Shah, P. Bennett, L. Cirignano, Y. Dmitriyev, M. Klugerman, K. Mandal, L. P. Moy, and R. A. Street, Mater. Res. Soc. Symp. Proc. **487**, 351 (1998).
- ⁹R. A. Street, S. E. Ready, F. Lemmi, K. S. Shah, P. Bennett, and Y. Dmitriyev, J. Appl. Phys. **86**, 2660 (1999).
- ¹⁰M. Schieber, A. Zuck, M. Braiman, J. Nissenbaum, R. Turchetta, W. Dulinski, D. Husson, and J. L. Riester, IEEE Trans. Nucl. Sci. **44**, 2571 (1997).
- ¹¹M. Schieber, H. Hermon, A. Zuck, A. Vilensky, L. Melekhov, R. Shatunovsky, and R. Turketa, Proc. SPIE **3768**, 296 (1999).
- ¹²R. Street, M. Mulato, M. Scheiber, H. Hermon, K. Shah, P. R. Bennett, Y. Dmitriyev, J. Ho, R. Lau, E. Meerson, S. E. Ready, B. Reisman, Y. Sado, K. van Schuylenbergh, A. Vilensky, and A. Zuck, Proc. SPIE **4320**, 1 (2001).
- ¹³H. Fujieta, IEEE Trans. Med. Imaging **11**, 34 (1992).
- ¹⁴A more detailed analysis of the charge collection as a function of absorption depth is given by S. Kasap, J. Phys. D **33**, 2853 (2000).
- ¹⁵M. Mulato, F. Lemmi, J. Ho, R. Lau, J. P. Lu, and R. Street, J. Appl. Phys. **90**, 1589 (2001).
- ¹⁶I. A. Cunningham, M. S. Westmore, and A. Fenster, Proc. SPIE **2432**, 143 (1995).
- ¹⁷J. H. Siewerdsen, L. E. Antonuk, Y. El-Mohri, J. Yorkston, W. Huang, J. M. Boudry, and I. A. Cunningham, Med. Phys. **24**, 71 (1997).
- ¹⁸L. E. Antonuk, K.-W. Jee, Y. El-Mohri, M. Maolinbay, S. Nassif, X. Rong, Q. Zhao, J. H. Siewerdsen, R. A. Street, and K. S. Shah, Med. Phys. **27**, 289 (2000).